Computational Materials Science 201 (2022) 110910

Contents lists available at ScienceDirect

Computational Materials Science

journal homepage: www.elsevier.com/locate/commatsci

Interphase effects on elastic properties of polymer nanocomposites reinforced by carbon nanocones

Seyed Saeid Taheri, Mir Masoud Seyyed Fakhrabadi *

School of Mechanical Engineering, College of Engineering, University of Tehran, Tehran, Iran

ARTICLE INFO

Keywords:
Carbon nanocones
Transversely isotropic behavior
Nanocomposite materials
Interphase regions

ABSTRACT

In this paper, interfacial and elastic properties of polymer-based nanocomposites reinforced by carbon nanocones (CNCs) are investigated. The CNCs are *transitional* structures from graphene to carbon nanotubes and, depending on their apex angles, show either more graphene or more nanotube behavior. Due to the importance of the interphase layer and its impact on the elastic properties of nanocomposites, the molecular dynamics method is used to investigate the behavior of polyethylene polymer in the interface of the CNCs. The MD simulation results reveal that there are two distinct interphase layers, i. e. the inner interphase region inside the CNCs and the outer interphase region outside the CNCs. While the outer interphase regions are the same in all cases, the size and properties of the inner interphase depend on the geometries of CNCs. Using the results of MD simulations, the finite element method is used to simulate CNC-reinforced polyethylene nanocomposites in larger dimensions. In finite element modeling, the effects of different orientations of nanofillers, various volume fractions, and geometrical parameters of the CNCs are studied.

1. Introduction

Due to their outstanding characteristics, carbon-based nanomaterials, e. g. graphene, fullerenes, and carbon nanotubes (CNTs) have been extensively used in nanocomposite reinforcement technology. The effect of carbon nanofillers on the electrical and mechanical enhancement of polymers is a well-studied subject in the literature [1–3]. Due to the morphology differences, fullerenes have different effects on the enhancement of nanocomposite properties compared to graphene, where the effect of 2D nanostructures is more notable than spherical ones [2]. Likewise, as tubular materials, CNTs have specific performance in the reinforcement of nanocomposites, which have been studied largely [3–7].

Based upon previous studies, it was proved that nanocomposite qualities are affected by the interphase layer; the region in which, due to the atomic and intermolecular interactions between matrix and nanofillers, densification of matrix phase leads to the further enhancement of nanocomposite properties [8]. Zare et al. [9] investigated the interphase characteristics in polymer-metal nanocomposites. Also, Ciprari *et al.* studied the reinforcement of polymer composites containing metal-oxide nanoparticles of alumina (Al_2O_3) and magnetite (Fe_3O_4) [10]. Eslami et al. investigated the interfacial behavior of polymer nanocomposites reinforced by Silica nanofillers using the molecular dynamic (MD) simulation method [11]. Their dynamic examination revealed that the results are dependent on the height scale, time scale, and temperature. Moreover, the effects of other nanoparticles such as clay [12] and ceramic [13] were also studied to determine their interphase properties.

The morphologies of nanoparticles have fundamental roles in the effectiveness of the interphase layer [14–16]. As a 2D material, the interfacial behavior of graphene was investigated using different methods, e. g. MD simulations [17–19], finite element method (FEM) [15,20], and experimental procedures [21]. In the case of tubular structures, the interfacial properties of CNTs have been studied via various approaches. The results revealed the importance of CNT geometries such as their heights, diameters, and volume fractions (VF) to reinforce the polymer nanocomposites [22,23]. Herasati et al. [8] performed a combination of MD and FEM simulations to characterize the interphase region in composites in which CNTs with various geometries were embedded in Polyvinylchloride (PVC) matrix. Besides, the notable impact of van der Waals (vdW) interactions on the results, they found that the number of CNT walls has a negligible effect on interphase qualities. Theoretically, some other research studies were conducted on interfacial mechanical and thermal enhancement of polymer

* Corresponding author.
E-mail address: mfakhrabadi@ut.ac.ir (M.M. Seyyed Fakhrabadi).

https://doi.org/10.1016/j.commatsci.2021.110910
Received 23 June 2021; Received in revised form 19 September 2021; Accepted 22 September 2021
Available online 30 September 2021

nanocomposites by coiled CNTs [24] and graphene spirals [25].

Having conical shapes, carbon nanocones (CNCs) can be classified into five different apex angles (Fig. 1) with variable properties ranging from graphene to CNTs [26,27]. Based on the exclusive possession of the mentioned precious qualities, they can be flexibly applied in highly efficient products [28]. Similar to other nanostructures, it is important to obtain their interfacial characteristics. Fakhrabadi and Khani [29] used FEM to study the interphase region in polymer nanocomposites reinforced by CNCs. In the current work, using the MD simulations, interphase properties of CNC-polyethylene (PE) nanocomposites are obtained. Furthermore, using the FEM, mechanical properties of the same composites were determined in larger dimensions.

2. Molecular dynamics simulations

To investigate interfacial effects on polymer-based nanocomposites, initial configurations of CNC structures embedded in PE molecules were made using Packmol [30]. Then, the main MD simulations were performed in the Large-scale Atomic/Molecular Massively Parallel Simulator (LAMMPS), where bonded and non-bonded atomic interactions were modeled by AIREBO potential function. Fig. 2 shows a model of representative volume element (RVE) containing PE molecules and CNC with 19.2° apex angle and 30 Å height in the final step of the simulation. In this case, CNCs with different apex angles as well as various heights were examined to evaluate the effects of the two mentioned geometrical parameters on interphase properties.

The RVE models were initially generated in larger simulation boxes in which the density of PE chains was 25% of normal condition. After equilibration of the systems, they were densified to reach the real density of PE (0.88 g/cm^3) using the *fix deform* command [31]. In this

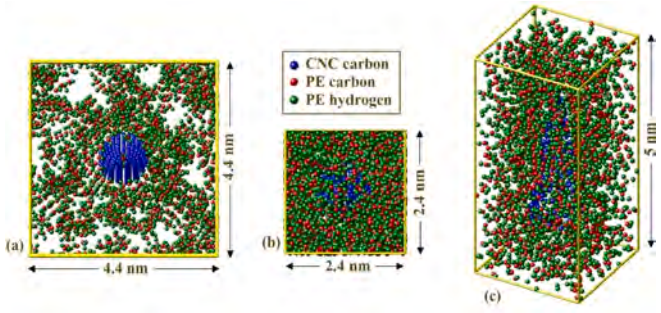

Fig. 2. Schematic representation of a CNC with 19.2° apex angle and 30 Å height embedded into PE matrix; (a) at the beginning of the simulation, and (b) upside view, and (c) 3D-view at end of the simulation.

procedure, all boundaries of the simulation box were shrunk until the final volume where the desired density was achieved. The dimension reduction rate was 1.25% per 10 ps at the temperature of 500 K and the pressure of 1 bar under NPT (constant number of particles, constant pressure, and constant temperature) ensemble. Consequently, the atomic system was cooled down to 300 K (room temperature) with the rate of 20 K for every 100 ps under the same ensemble. Finally, the RVE structure was thermally equilibrated at room temperature for 1 ns under NVT (constant number of particles, constant volume, and constant temperature) ensemble.

To determine the properties of the interphase layer, all space of RVE was divided into smaller chunks. Due to the conical shape of CNCs, the chunks were considered to be cylindrical regions, therefore the variation of PE density through the RVE space can be analyzed in both radial and

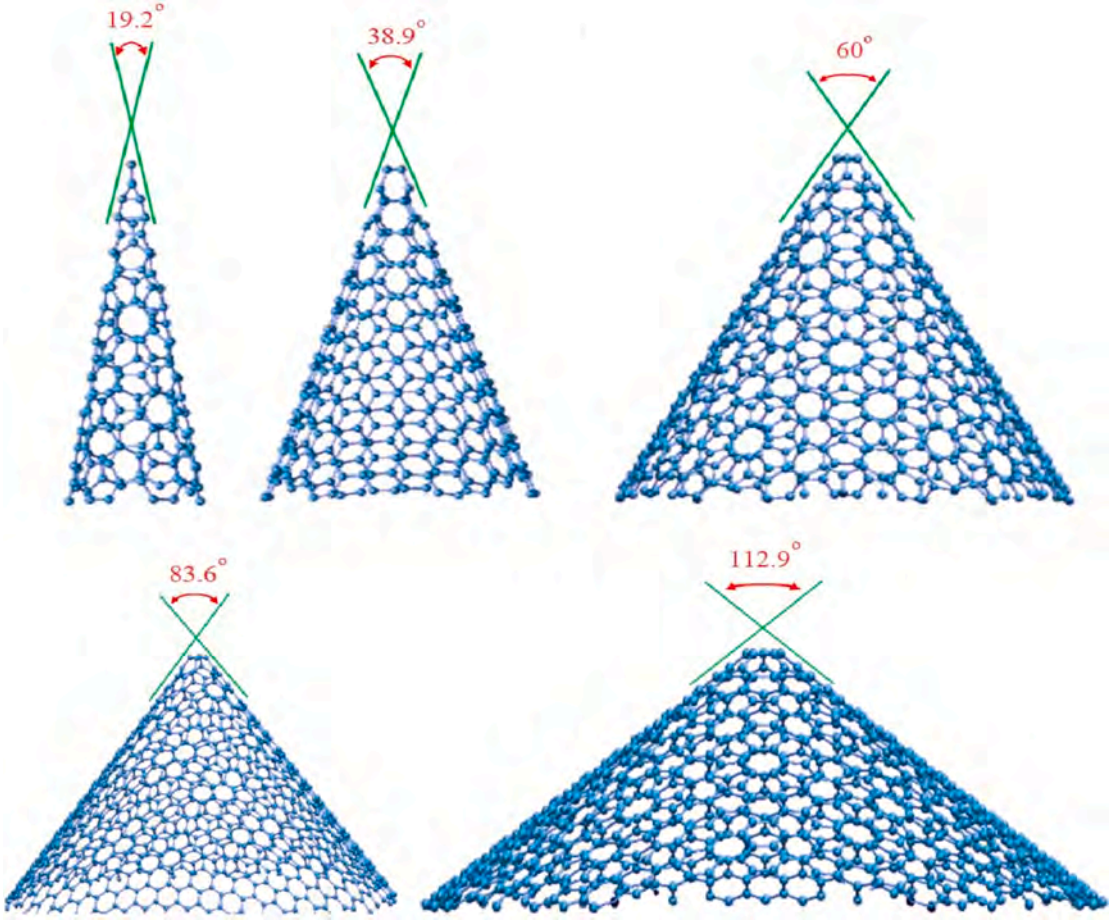

Fig. 1. Classification of CNCs in five apex angles.

axial directions.

According to Fig. 3, the simulation of composites reinforced by wider CNCs is required to perform very time-consuming calculations. Thus, interfacial properties of CNCs with 83.6° and 112.9° apex angles were investigated with only a height of 10 Å. However, for other apex angles, the effects of the height variation were considered.

3. Finite element simulations

In this section, the mechanical properties of polymer nanocomposites are determined using (FEM). Having used the results of the previous section (MD method) on the density variation of the polymer and correlating it to the experimentally measured elastic modulus of PE vs. its density that is available in the literature [32], the effect of interphase layer on reinforcement of PE-CNC nanocomposites is studied. The interphase regions are considered as high-density polyethylene (HDPE). According to [32], as the density of PE increases, it becomes stiffer and its Young's modulus increases [32]. Hence, the elastic coefficients corresponding to the density of each region (provided in Table 1) are considered in the FE modeling. This approach was used before in some studies on the mechanical analysis of polymer nanocomposites [8,33].

The FE-based analysis of RVEs was studied using ABAQUS software [34] as well as scripting in Python package [35], where it was essential to investigate various nano-fillers distributions. PE has a density of 0.88 g/cm^3 [36] and Young's modulus of 800 MPa [32], while it becomes stiffer as its density increases. Therefore, using the results available in the literature, the interphase regions are considered as high-density polyethylene (HDPE) with higher Young's modulus [32]. Table 1 presents the elastic coefficients defined in the FE modeling corresponding to the density of each region.

In our previous study [26], we proved that CNCs have transversely isotropic elastic properties with five independent constants. Hence, to define the elastic properties of CNCs in FE software, we used the elastic constants (see Table 2) that we obtained before [26]. By considering Y-axis as the axial direction of CNCs, E_2 is axial Young's modulus and, due to the transversely isotropic behavior of CNCs, the two transverse components (E_1, E_3) have the same values. Also, G and ν are referred to the shear modulus and Poisson's ratio.

Fig. 4 illustrates different orientations of CNCs inside the matrix and different loading directions. In Fig. 4a all CNCs are oriented along the tension direction of the RVE while Fig. 4b presents randomly oriented nanofillers in the RVE. Furthermore, Fig. 4 c and d demonstrate the transverse loading directions. Due to their geometries and non-isotropic elastic behavior, it is predicted that CNC orientations and the loading directions will affect the enhancement of elastic properties of the matrix.

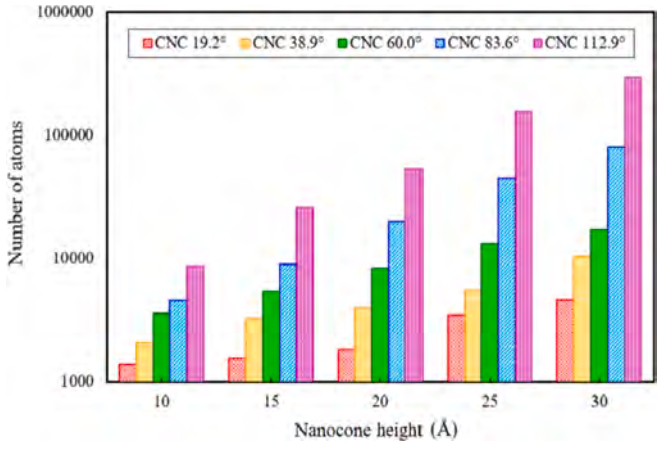

Fig. 3. The number of atoms in simulations vs. geometrical parameters of CNCs.

Table 1
Elastic moduli of polymer phases based on their density [32].

Phase	Density (g/cm^3)	Young's modulus (GPa)	Poisson's ratio
Bulk matrix	0.88	0.8	0.4
Outer interphase	0.94	1	0.4
Inner interphase	1.02	1.1	0.4
	1.05	1.2	0.4
	1.1	1.3	0.4
	1.2	1.4	0.4

Table 2
Transversely isotropic elastic constants of CNCs vs. their apex angles and heights [26].

Angle-height	E_1, E_3(GPa)	E_2(GPa)	ν_{21}, ν_{23}	ν_{13}	G_{21}, G_{23}(GPa)
19.2° – 10 Å	444.5	860.5	0.16	0.25	147.8
19.2° – 20 Å	414.3	849.7	0.16	0.26	148
19.2° – 30 Å	398.5	803.6	0.16	0.25	150.4
38.9° – 10 Å	572.9	732.5	0.14	0.22	136.4
38.9° – 20 Å	505.3	702.5	0.14	0.18	136.5
38.9° – 30 Å	471.6	654.5	0.14	0.19	136.1
60° – 10 Å	698.3	549.5	0.11	0.17	131.2
60° – 20 Å	623.5	516.4	0.11	0.15	130
60° – 30 Å	574.4	485.1	0.11	0.18	129.7

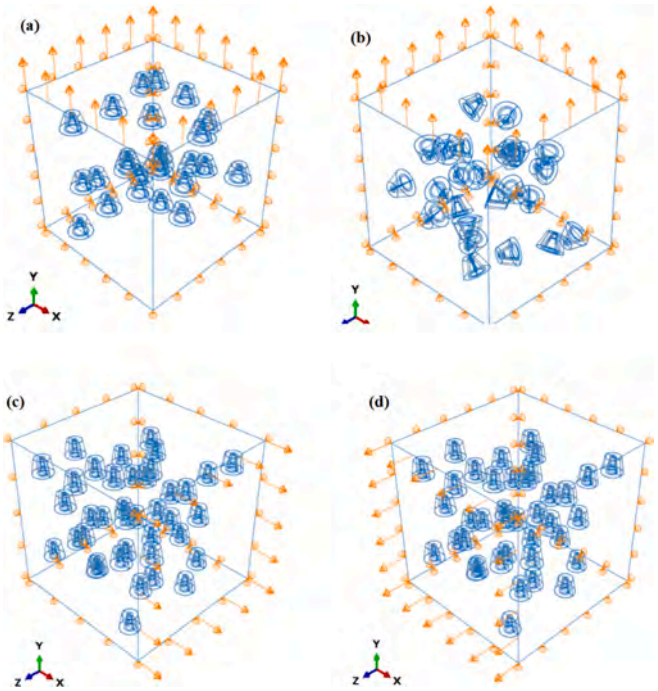

Fig. 4. (a) Loading direction along with CNC orientation, (b) random orientation of CNC inside the matrix, (c) and (d) transverse loadings on the CNCs. The VF is considered 0.5%.

To mesh the RVEs, tetrahedron elements with free meshing were applied. Loadings were performed with a strain of 0.001 in all cases. Fig. 5 shows the displacement contour of RVE in the mentioned strain, where the RVE dimension is 30 nm. This value is ten times larger than the largest dimension of CNC (3 nm). Determination of Young's modulus is done based on linear Hook's law:

$$\sigma = E\varepsilon \tag{1}$$

where σ and ε are the volumetric averages of stress and strain of all elements, formulated in Eqs. (2) and (3), respectively.

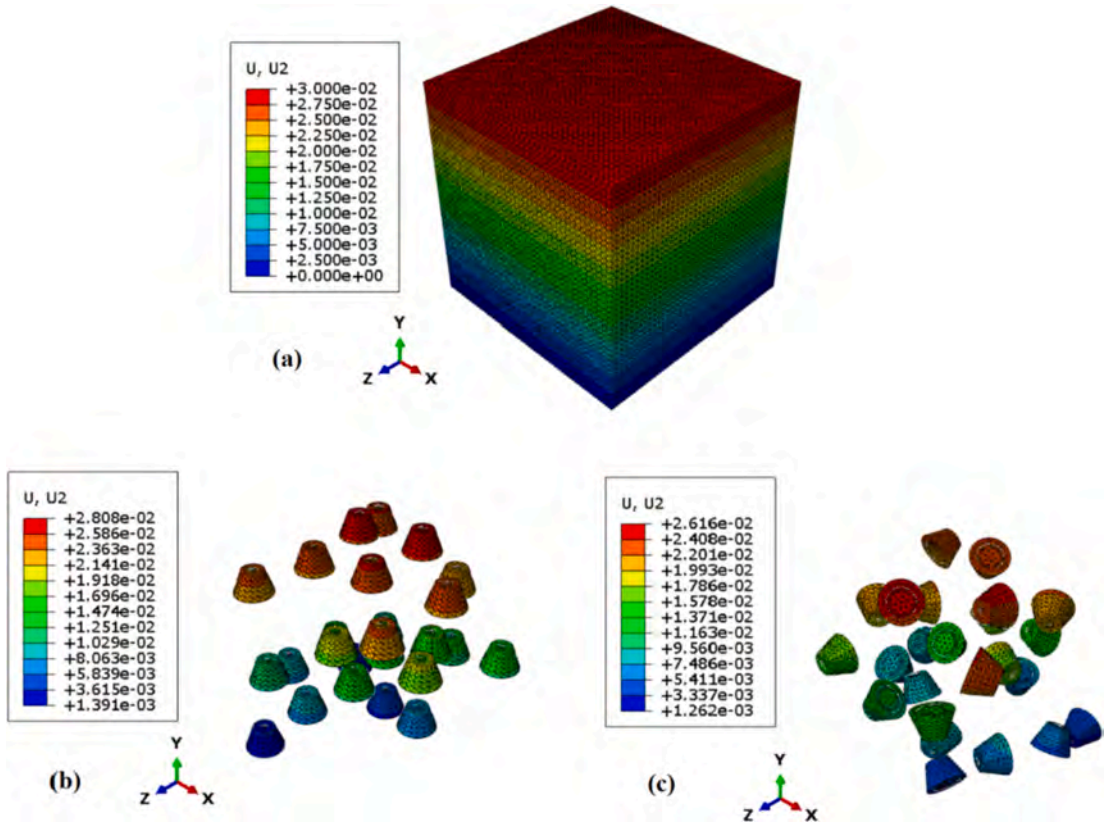

Fig. 5. Displacement contour of (a) RVE with (b) oriented, and (c) randomly distributed nanofillers.

$$\sigma = \frac{1}{V}\int_V \sigma_e \mathrm{dv} \tag{2}$$

$$\varepsilon = \frac{1}{V}\int_V \varepsilon_e \mathrm{dv} \tag{3}$$

where V is the RVE volume, and σ_e and ε_e are stress and strain of each element.

The other elastic constant, Poisson's ratio, ν, was obtained based on Eq. (4).

$$\nu = -\frac{\varepsilon^{'}}{\varepsilon} \tag{4}$$

where $\varepsilon^{'}$ is the circumferential strain of the RVE.

4. Results and discussion

4.1. MD results

The MD simulation of interfacial behavior of CNC-based polymer nanocomposites reveals that the density of the polymer phase around the nanofillers is not constant. The density of PE matrix depends on the distance from the CNC. At the vicinity of the CNC wall, the density remarkably increases. Interestingly, the density of the HDPE inside the CNCs is higher than the outer side. This leads to having two distinct interphase regions: inner interphase and outer interphase. Therefore, an RVE contains four main regions, i.e. CNC, bulk matrix, inner interphase, and outer interphase (see Fig. 6).

According to the results presented in Fig. 7(a–c), radial variation of PE density outside of the CNC is effectively independent of the CNC height. Also, based on the result shown in Fig. 7(d), the matrix density outside the CNC does not depend on the apex angle, considerably. As a result, in the thickness and density cases, it can be concluded that the

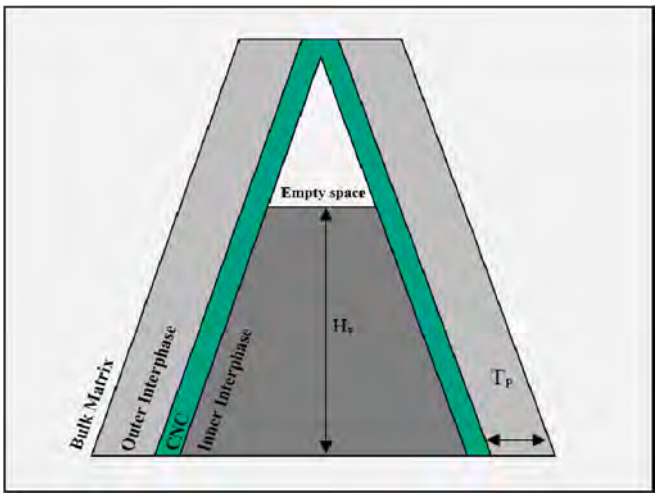

Fig. 6. Schematic representation of the axial section of a CNC with its interfacial regions.

outer interphase's properties (thickness and density) are not a function of the CNC height and apex angle. Another noticeable finding is the fluctuation of density along the radial direction where the density soars to almost 3 g/cm^3, and then, plummets to the lowest point. Finally, after a few peaks and valleys, it becomes stable around the density of bulk PE. The thickness of the unstable region (Tp) can be considered as the thickness of the outer interphase, which is almost 9 Å. Also, the average density of PE in this region can be considered as the interphase density [8].

Variation of density vs. time is provided in Fig. 8. Very similar trends are observed for the results during the period of 2 ps and the

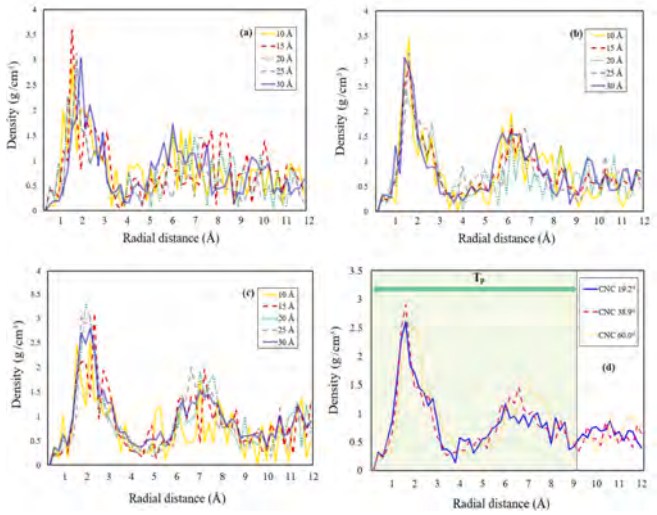

Fig. 7. Variation of the local density of PE along the radial direction of (a) 19.2°, (b) 38.9°, and (c) 60.0° CNCs with different heights (10–30 Å), (d) average density of apex angle groups.

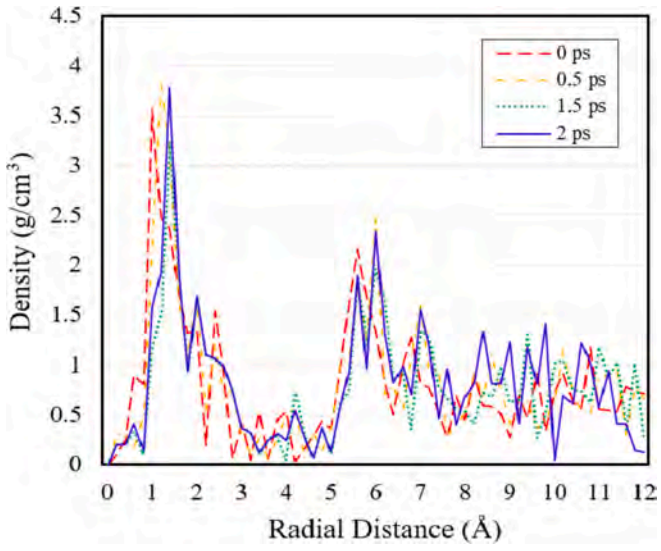

Fig. 8. Convergence of PE density vs time.

convergence of the results with time is clear. The mean squared error (MSE) between the density of each time-step and the final time-step, i. e. 2 ps shows a monotone reduction (from 0.312 to 0.199 and then to 0.110) which quantitatively proves the convergence.

To prove the accuracy and determine the effects of the unit cell size on the results, two unit cells with different dimensions are simulated. The comparison presented in Fig. 9 reveals that from about 8 Å to the end, we reached the bulk polymer density and the larger unit cell size does not affect the results because the interphase region is already inside the smaller unit cell.

Fig. 10 indicates that the density of the outer interphase is constant in all cases equaling 0.94 g/cm^3. In the case of inner interphase, the results of two CNCs with the apex angles of 38.9° and 60° presented in Fig. 11(a) reveal that the density of PE in this region is considerably dependent on geometrical parameters of the CNCs, where sharper ones have higher density but as their heights increase, the density decreases. In detail, the inner interphase of the 38.9° CNC with 10 Å has a density of almost 1.25 g/cm^3. However, as its height increases the density decreases so that the same CNC with 30 Å has a density around 1.2 g/cm^3.

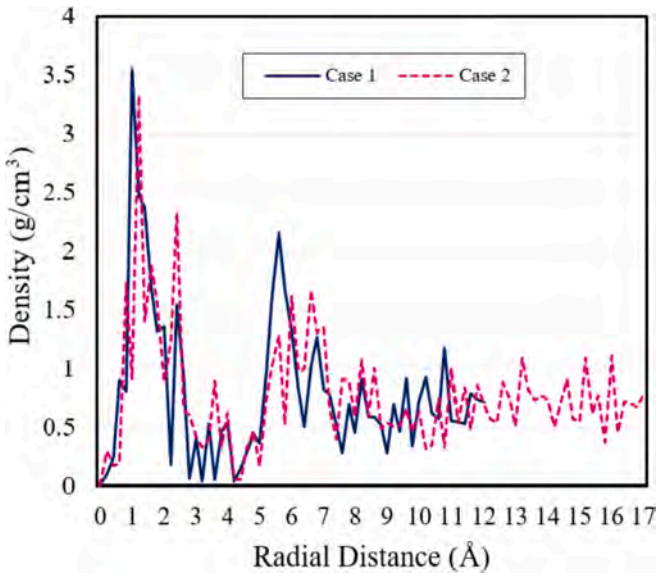

Fig. 9. Effects of the unit cell size on PE density in two RVE cases of 38.9° CNC.

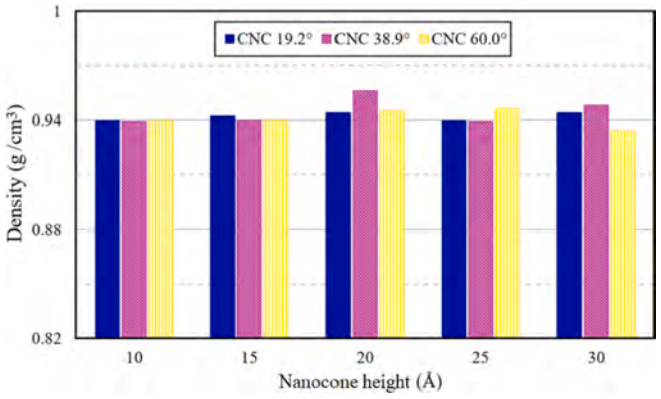

Fig. 10. The density of outer interphase vs. apex angles and heights of CNCs.

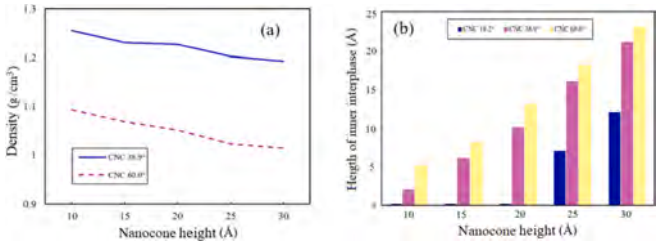

Fig. 11. The density of inner interphase vs. apex angles and heights of CNCs, (b) Height of inner interphase vs. apex angles and heights of CNCs.

Following the same trend, the interphase density of 60° CNCs varies from 1.1 g/cm^3 to 1 g/cm^3 as their heights grow from 10 Å to 30 Å. Obviously, as the heights and apex angles of the CNCs increase, the heights of their interphase increase (Fig. 11(b)). It is worth noting that, due to repulsive forces, the PE chains cannot penetrate the short CNCs with the 19.2° apex angle. In other words, the base diameters of the CNCs must be large enough to provide a situation in which PE molecules can overcome the energy barrier to enter the CNC. Therefore, those shorter than 25 Å do not have an inner interphase layer. The obtained inner interphase densities of 19.2° CNCs with heights of 25 Å and 30 Å are equal to 1.421, 1.374, respectively which are consistent with the results presented in Fig. 11(a).

As mentioned before, since the investigation of interfacial behavior of wider CNCs is very time-consuming due to their very large number of atoms, we studied only the shortest ones (with 10 Å height). The results are presented in Table 3.

4.2. FEM results

Finite element modeling of RVEs requires verification of the results in the case of accuracy in the number and size of meshes. Thus, the refinement of mesh is performed, and the satisfying convergent results are presented in Fig. 12. There were used four levels of mesh sizes including coarse (45000 elements), medium (70000 elements), fine (200000 elements), and very fine (400000 elements). As mentioned before, the determination of Young's modulus of RVE is done based upon linear elastic Hook's law; an equation in which the stress and strain of all elements are required. Fig. 13(a–c) illustrates the stress contours in an arbitrary CNC and its outer and inner interphase regions. Since CNC has a higher elastic modulus, it sustains higher stresses than the two other regions (see stress magnitude of each phase). In addition, the stress and strain contours of the nanocomposite RVE with oriented 38.9° CNCs are depicted in Fig. 13(d, e).

The enhancement of elastic properties of PE-CNC nanocomposites is studied in different cases such as the geometrical parameters of CNCs (height and apex angle), their orientation, and VF of the nanocomposite. VF is considered as the ratio of CNC volume to the RVE volume:

$$VF = \frac{V_{CNC}}{V_{RVE}} \tag{5}$$

Finally, with the use of the Query toolset in the Visualization module of Abaqus [37], the VF of each region was also calculated according to the volume of corresponding instances, where the results well agreed with the assigned ratios from Eq. (5). The results illustrated in Fig. 14(a, b) reveal that RVEs of oriented 19.2° CNCs (0.5% VF) with 30 Å height have the highest Young's modulus (841 MPa). This means that as the apex angle increases, Young's modulus of nanocomposites decreases, where RVEs of 38.9° and 60° CNCs are less strengthened (about 3.5%). Interestingly, as the apex angle of CNCs increases, the VF of the inner interphase increases (see Fig. 14b). This affects the enhancement of the polymer positively which is against the effect of apex angles.

Moreover, as shown in Fig. 14(c), as their height increases, CNCs are more effective to reinforce the polymer, while longer ones have lower Young's modulus [26]. This phenomenon is due to the increase of the VF of interphase regions (see Fig. 14c). In other words, although the elastic properties of CNCs decrease as their heights increase, their corresponding interphase regions become larger in RVE. Thus, a larger space of the RVE is occupied by HDPE with a higher elastic modulus.

To validate the results, we followed the process explained in [38] and built both FEM (Fig. 15) and MD unit cells of three different apex angles and compared the outcomes of elastic modulus. Fig. 15 shows the loading, strain, and stress of the unit cell obtained from FE modeling. The same loading was applied on the MD unit cell introduced before in Fig. 2.

Fig. 16 presents the comparison of the effective elastic modulus of single-fiber (4% VF) unit cells obtained from MD simulations and FEM. The results show good agreements with the largest deviation of 4.3% between the two methods which is acceptable for engineering tasks.

In Fig. 17, the enhancement of the elastic modulus of

Table 3
Interfacial properties of PE at the vicinity of the two widest CNCs with 10 Å height.

Apex angle	Outer interphase density (g/cm^3)	Inner interphase density (g/cm^3)	Height of inner interphase (Å)
83.6°	0.948	1.076	5
112.9°	0.946	1.024	7

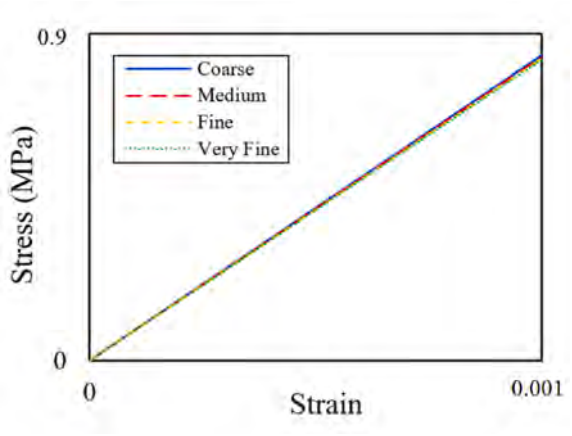

Fig. 12. Stress-strain curves of different mesh sizes.

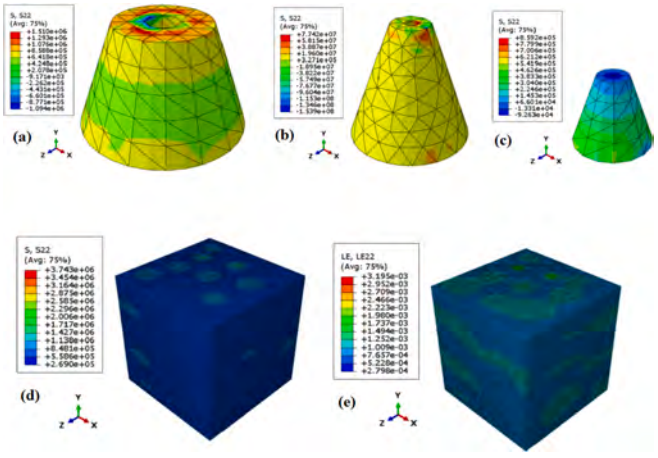

Fig. 13. Stress contours of (a) outer interphase, (b) CNC, and (c) inner interphase. (d) Stress and (e) strain contours of RVE with oriented 38.9° CNCs.

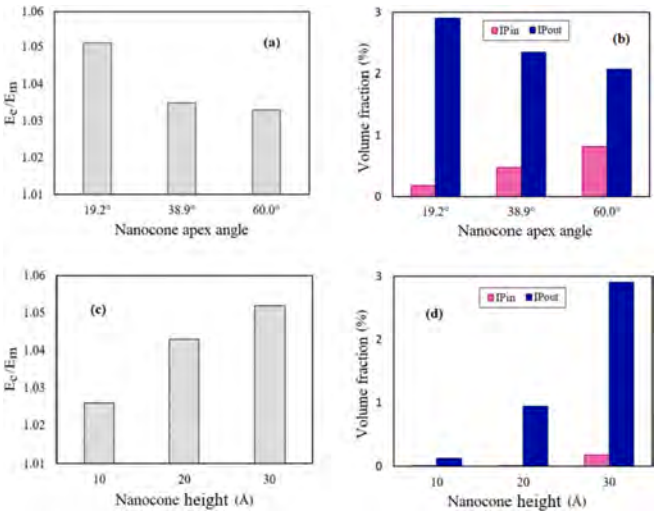

Fig. 14. The effects of apex angles of oriented (0.5% volume fraction) CNCs with 30 Å height on (a) enhancement of Young's modulus ratio of nanocomposite (E_c) over pure polymer (E_m) in CNCs' axial directions, and (b) the volume fraction of interfacial regions. The effects of height of oriented (0.5% volume fraction) CNCs with 19.2° apex angle on (c) enhancement of elastic constant of PE, and (d) the volume fraction of interfacial regions.

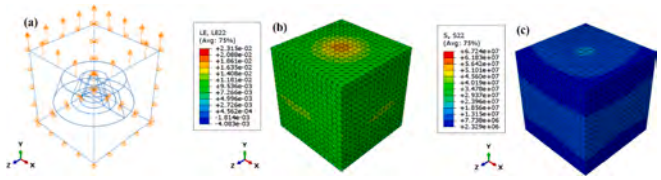

Fig. 15. FE modeling of the unit cell with single CNC fiber; (a) boundary conditions and loading, (b) strain contour, and (c) stress contour.

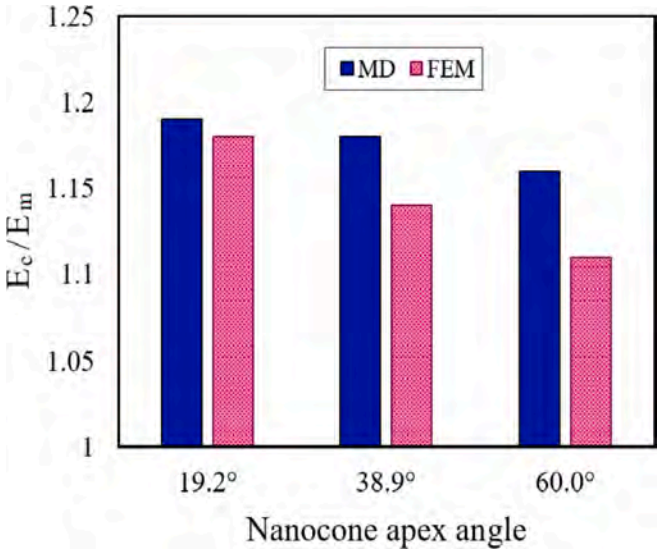

Fig. 16. Comparison of the effective elastic modulus of single fiber (4%VF) unit cells obtained from MD and FE methods.

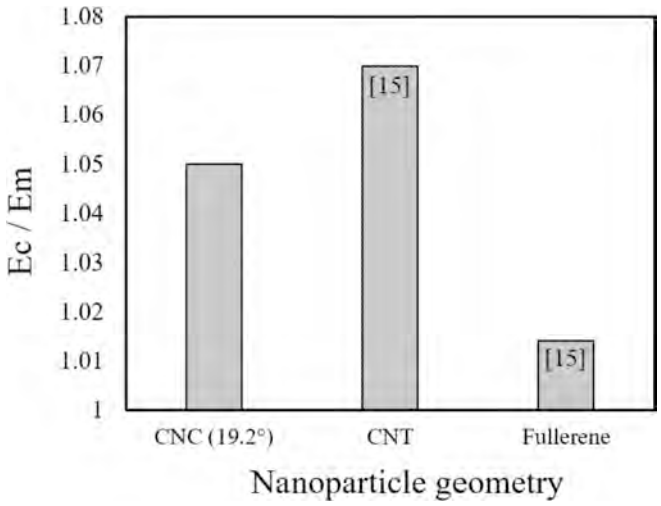

Fig. 17. Comparison of the effective elastic moduli of PE nanocomposites of different carbon nanoparticles (1% VF) [15].

nanocomposites reinforced with CNC (with 19.2° apex angle and 10 Å length) determined in this study is compared with some other carbon-based nanoparticles from the literature [15]. In all cases, the VF is 1%. The results are in the same ranges but due to the lower elastic modulus of the CNCs than the CNTs, the former has a bit lower modulus ratio than the latter. Fullerene has the smallest effect.

The effects of VFs and orientations of CNCs are presented in Fig. 18. As expected, an increase in VF of CNCs leads to higher elastic properties, where RVEs with 0.5% CNCs have about 805 MPa, while those with 1% and 1.5% CNCs have almost 815 MPa and 822 MPa, respectively. Furthermore, in RVEs of randomly distributed CNCs, it seems that they tend to have isotropic elastic behavior. In other words, since CNCs are transversely isotropic materials, the elastic behavior of RVEs is substantially dependent on the distribution of the nanoparticles. It means that with randomly distributed nanofillers, the elastic modulus of RVEs should be constant in all directions. Also, in higher VFs, this similarity should become more prominent. The results of Fig. 18 prove this assumption, where elastic constants in the RVE with 1.5% VF CNCs are the most convergent results (lower than 0.3% diversity).

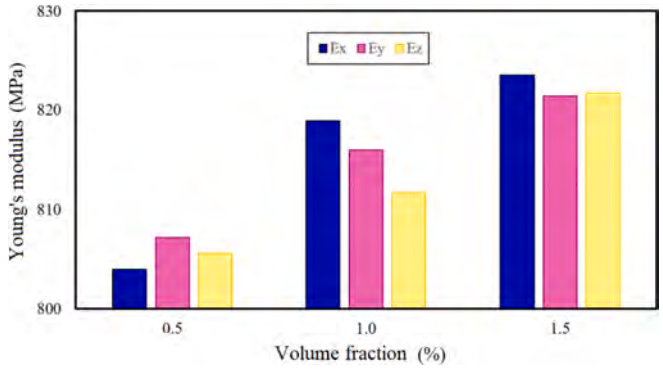

Fig. 18. The effect of VF of 38.9° CNC with 30 Å height on Young's modulus components of the RVE.

On the other hand, as shown in Table 4, RVEs with oriented nanofibers tend to behave as transversely isotropic materials. This is based on two reasons; the orientation of nanofibers, and their transversely isotropic behavior. Aligned CNCs along with the Y-direction led to the situations in which RVEs have larger elastic constants in this direction, while in the two other directions, they are almost the same.

As another important elastic coefficient, Poisson's ratio is also determined in this work. Similar to the elastic modulus, Poisson's ratio is also dependent on the apex angles of CNCs. As shown in Fig. 19, RVEs with oriented nanofillers have two same Poisson's ratios in x-y and y-z planes unequal to the circumferential component (υ_{13}).

5. Conclusions

In this paper, based on the MD simulations and FEM, the interfacial behavior of polyethylene in the vicinity of CNCs and its impact on the enhancement of CNC-PE nanocomposites were studied. First, the MD simulation method was used to obtain the properties of the interphase layer inside and outside of the CNCs used to reinforce polymer nanocomposites. Subsequently, the MD results were fed into the FE software to investigate the elastic properties of nanocomposite RVEs. The effects of the geometrical parameters of the CNCs were analyzed in both methods. Also, the impacts of various VFs and orientations of the nanofillers on the elastic properties of the polymer nanocomposites were studied. The main outcomes are summarized below:

I. Due to the conical shapes of nanoparticles, there are two inner and outer interphase regions with different polymer condensation and elastic properties.

Table 4
Young's modulus of RVEs (0.5% VF) with oriented CNCs along Y-direction.

Apex angles	E1 (MPa)	E2 (MPa)	E3 (MPa)
19.2°	822.2	841.3	822.3
38.9°	822	827.7	822
60°	830.3	827.9	830.3

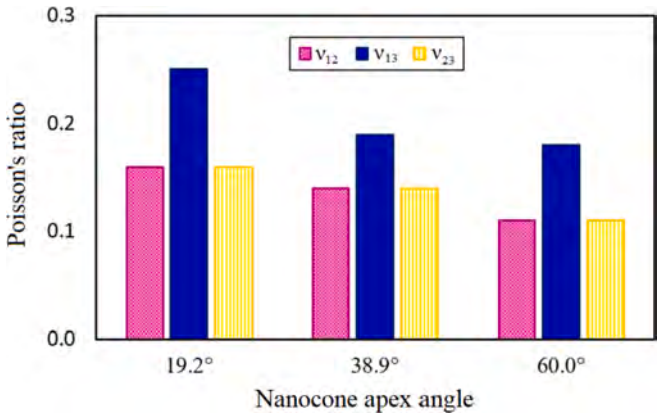

Fig. 19. Poisson's ratios of RVEs vs. the apex angles of CNCs.

II. The properties of the outer interphase are independent of the CNC apex angles and heights, while the inner interphase is highly dependent on both geometrical parameters.
III. The density of the inner interphase region increases in shorter and sharper CNCs.
IV. Although Young's modulus of CNCs decrease as their height increases, RVEs of longer CNCs have higher elastic constants.
V. RVEs with more embedded CNCs are elastically stronger.

6. Data availability

The raw/processed data required to reproduce these findings cannot be shared at this time as the data also forms part of an ongoing study.

CRediT authorship contribution statement

Seyed Saeid Taheri: Methodology, Software, Formal analysis, Investigation, Data curation, Writing – original draft, Visualization. **Mir Masoud Seyyed Fakhrabadi:** Conceptualization, Methodology, Formal analysis, Data curation, Writing – review & editing, Project administration, Supervision, Funding acquisition.

Declaration of Competing Interest

The authors declare that they have no known competing financial interests or personal relationships that could have appeared to influence the work reported in this paper.

References

[1] Y. Li, X. Huang, L. Zeng, R. Li, H. Tian, X. Fu, Y.u. Wang, W.-H. Zhong, A review of the electrical and mechanical properties of carbon nanofiller-reinforced polymer composites, J. Mater. Sci. 54 (2) (2019) 1036–1076, https://doi.org/10.1007/s10853-018-3006-9.
[2] C.-T. Lu, A. Weerasinghe, D. Maroudas, A. Ramasubramaniam, A comparison of the elastic properties of graphene- and fullerene-reinforced polymer composites: the role of filler morphology and size, Sci. Rep. 6 (1) (2016), https://doi.org/10.1038/srep31735.
[3] W. Bauhofer, J.Z. Kovacs, A review and analysis of electrical percolation in carbon nanotube polymer composites, Compos. Sci. Technol. 69 (10) (2009) 1486–1498, https://doi.org/10.1016/j.compscitech.2008.06.018.
[4] Z. Han, A. Fina, Thermal conductivity of carbon nanotubes and their polymer nanocomposites: a review, Prog. Polym. Sci. 36 (7) (2011) 914–944, https://doi.org/10.1016/j.progpolymsci.2010.11.004.
[5] R.F. Gibson, E.O. Ayorinde, Y.-F. Wen, Vibrations of carbon nanotubes and their composites: a review, Compos. Sci. Technol. 67 (1) (2007) 1–28, https://doi.org/10.1016/j.compscitech.2006.03.031.
[6] G. Mittal, V. Dhand, K.Y. Rhee, S.-J. Park, W.R. Lee, A review on carbon nanotubes and graphene as fillers in reinforced polymer nanocomposites, J. Ind. Eng. Chem. 21 (2015) 11–25, https://doi.org/10.1016/j.jiec.2014.03.022.
[7] P.J.F. Harris, Carbon nanotube composites, Int. Mater. Rev. 49 (1) (2004) 31–43, https://doi.org/10.1179/095066004225010505.
[8] S. Herasati, L.C. Zhang, H.H. Ruan, A new method for characterizing the interphase regions of carbon nanotube composites, Int. J. Solids Struct. 51 (9) (2014) 1781–1791, https://doi.org/10.1016/j.ijsolstr.2014.01.019.
[9] Y. Zare, Effects of interphase on tensile strength of polymer/CNT nanocomposites by Kelly-Tyson theory, Mech. Mater. 85 (2015) 1–6, https://doi.org/10.1016/j.mechmat.2015.02.002.
[10] D. Ciprari, K. Jacob, R. Tannenbaum, Characterization of polymer nanocomposite interphase and its impact on mechanical properties, Macromolecules 39 (19) (2006) 6565–6573, https://doi.org/10.1021/ma0602270.
[11] H. Eslami, M. Rahimi, F. Müller-Plathe, Molecular dynamics simulation of a silica nanoparticle in oligomeric poly(methyl methacrylate): a model system for studying the interphase thickness in a polymer-nanocomposite via different properties, Macromolecules 46 (21) (2013) 8680–8692, https://doi.org/10.1021/ma401443v.
[12] S.P. Davtyan, A.O. Tonoyan, A.A. Tataryan, C. Schick, Interphase phenomena in superconductive polymer-ceramic nanocomposites, Compos. Interfaces 13 (4-6) (2006) 535–544, https://doi.org/10.1163/156855406777408502.
[13] Y. Zare, H. Garmabi, Thickness, modulus and strength of interphase in clay/polymer nanocomposites, Appl. Clay Sci. 105–106 (2015) 66–70, https://doi.org/10.1016/j.clay.2014.12.016.
[14] J. Choi, H. Shin, S. Yang, M. Cho, The influence of nanoparticle size on the mechanical properties of polymer nanocomposites and the associated interphase region: a multiscale approach, Compos. Struct. 119 (2015) 365–376, https://doi.org/10.1016/j.compstruct.2014.09.014.
[15] B. Mortazavi, J. Bardon, S. Ahzi, Interphase effect on the elastic and thermal conductivity response of polymer nanocomposite materials: 3D finite element study, Comput. Mater. Sci. 69 (2013) 100–106, https://doi.org/10.1016/j.commatsci.2012.11.035.
[16] B. Mortazavi, M. Baniassadi, J. Bardon, S. Ahzi, Modeling of two-phase random composite materials by finite element, Mori-Tanaka and strong contrast methods, Compos. Part B Eng. 45 (1) (2013) 1117–1125, https://doi.org/10.1016/j.compositesb:2012.05.015.
[17] M. Wang, C. Yan, Atomistic simulation of interfacial behaviour in graphene-polymer nanocomposite, Sci. Adv. Mater. 6 (7) (2014) 1501–1505, https://doi.org/10.1166/sam.2014.1810.
[18] Y. Zhang, X. Zhuang, J. Muthu, T. Mabrouki, M. Fontaine, Y. Gong, T. Rabczuk, Load transfer of graphene/carbon nanotube/polyethylene hybrid nanocomposite by molecular dynamics simulation, Compos. Part B Eng. 63 (2014) 27–33, https://doi.org/10.1016/j.compositesb:2014.03.009.
[19] A. Alizadeh Sahraei, A.H. Mokarizadeh, D. George, D. Rodrigue, M. Baniassadi, M. Foroutan, Insights into interphase thickness characterization for graphene/epoxy nanocomposites: a molecular dynamics simulation, Phys. Chem. Chem. Phys. 21 (36) (2019) 19890–19903, https://doi.org/10.1039/C9CP04091A.
[20] G.I. Giannopoulos, I.G. Kallivokas, Mechanical properties of graphene based nanocomposites incorporating a hybrid interphase, Finite Elem. Anal. Des. 90 (2014) 31–40, https://doi.org/10.1016/j.finel.2014.06.008.
[21] H. Yang, F. Cai, Y. Luo, X. Ye, C. Zhang, S. Wu, The interphase and thermal conductivity of graphene oxide/butadiene-styrene-vinyl pyridine rubber composites: a combined molecular simulation and experimental study, Compos. Sci. Technol. 188 (2020) 107971, https://doi.org/10.1016/j.compscitech.2019.107971.
[22] J. Amraei, J.E. Jam, B. Arab, R.D. Firouz-Abadi, Modeling the interphase region in carbon nanotube-reinforced polymer nanocomposites, Polym. Compos. 40 (S2) (2019) E1219–E1234, https://doi.org/10.1002/pc.v40.s210.1002/pc.24950.
[23] S. Yang, S. Yu, W. Kyoung, D.-S. Han, M. Cho, Multiscale modeling of size-dependent elastic properties of carbon nanotube/polymer nanocomposites with interfacial imperfections, Polymer (Guildf) 53 (2) (2012) 623–633, https://doi.org/10.1016/j.polymer.2011.11.052.
[24] A. Kianfar, M.M. Seyyed Fakhrabadi, M.M. Mashhadi, Prediction of mechanical and thermal properties of polymer nanocomposites reinforced by coiled carbon nanotubes for possible application as impact absorbent, Proc. Inst. Mech. Eng. Part C J. Mech. Eng. Sci. 234 (4) (2020) 882–902, https://doi.org/10.1177/0954406219885969.
[25] S. Norouzi, A. Kianfar, M.M.S. Fakhrabadi, Multiscale simulation study of anisotropic nanomechanical properties of graphene spirals and their polymer nanocomposites, Mech. Mater. 145 (2020) 103376, https://doi.org/10.1016/j.mechmat.2020.103376.
[26] S.S. Taheri, M.M. Seyyed Fakhrabadi, Molecular dynamics simulation of transversely isotropic elastic properties of carbon nanocones, Phys. Scr. 96 (3) (2021) 035702, https://doi.org/10.1088/1402-4896/abd5ed.
[27] D. Ma, H. Ding, X. Wang, N. Yang, X. Zhang, The unexpected thermal conductivity from graphene disk, carbon nanocone to carbon nanotube, Int. J. Heat Mass Transf. 108 (2017) 940–944, https://doi.org/10.1016/j.ijheatmasstransfer.2016.12.092.
[28] W. Li, W. Wang, Y. Zhang, Y. Yan, P. Král, J. Zhang, Highly efficient water desalination in carbon nanocones, Carbon N. Y. 129 (2018) 374–379, https://doi.org/10.1016/j.carbon.2017.12.039.
[29] M.M. Seyyed Fakhrabadi, N. Khani, Investigation of interphase effects on mechanical behaviors of carbon nanocone-based composites, Mech. Ind. 15 (4) (2014) 287–292, https://doi.org/10.1051/meca/2014038.
[30] http://m3g.iqm.unicamp.br/packmol/home.shtml, (2020).
[31] https://lammps.sandia.gov/doc/fix_deform.html, (2020).
[32] Y. Zhang, D. Rodrigue, A. Ait-Kadi, High density polyethylene foams. II. Elastic modulus, J. Appl. Polym. Sci. 90 (8) (2003) 2120–2129, https://doi.org/10.1002/(ISSN)1097-462810.1002/app.v90:810.1002/app.12822.
[33] A. Shahrokh, M.M. Seyyed Fakhrabadi, Effects of copper nanoparticles on elastic and thermal properties of conductive polymer nanocomposites, Mech. Mater. 160 (2021) 103958, https://doi.org/10.1016/j.mechmat.2021.103958.

[34] ABAQUS, Abaqus 6.19, Dassault Systèmes Simulia Corp., Provid. RI, USA. (2019).
[35] Abaqus Scripting User's Guide, n.d. http://130.149.89.49:2080/v6.13/books/cmd/default.htm.
[36] K. Batra, Role of additives in linear low density polyethylene films, (2014). https://www.slideshare.net/kamalbatra111/polyethylene-pe.
[37] Querying the model in the Visualization module, n.d. http://130.149.89.49:2080/v6.13/books/usi/default.htm.
[38] G.I. Giannopoulos, Linking MD and FEM to predict the mechanical behaviour of fullerene reinforced nylon-12, Compos. Part B Eng. 161 (2019) 455–463, https://doi.org/10.1016/j.compositesb:2018.12.110.